THREE-DIMENSIONAL PARTICLE SIMULATION OF GRID EROSION IN ION THRUSTERS

Xiaohang Peng*, Wilhelmus M. Ruyten**, and Dennis Keefer†
Center for Space Transportation and Applied Research and
University of Tennessee Space Institute
Tullahoma, Tennessee 37388

Abstract

A particle simulation computational code has been developed to study the effect of charge exchange induced grid erosion in ion engines. The code is based on the particle-in-cell (PIC) method to calculate the ion flow and a Monte Carlo method to calculate the charge exchange collisions. Both two- and three-dimensional versions of this code have been developed. The three- diemnsional version has successfully predicted the experimentally observed erosion pattern, where maximum erosion occurs at the geometric center of the accelerator grid apertures. The two-diemnsional version of the code has been used to evaluate the influence of the assumed downstream boundary condition on the predicted potential field downstream of the accelerator grid. The predicted potential field was found to be insensitive to the choice of boundary condition when the boundary condition was placed far enough downstream of the accelerator grid.

I. Introduction

Serious accelerator grid sputtering erosion has been observed during long term tests of ion engines in ground test facilities [1-3]. It is well known that this accelerator grid sputtering erosion is caused by the formation of charge exchange ions. These charge exchange ions are created by charge exchange collisions between the fast beam ions and neutral atoms. Since the ion source can not be perfect, it will always have some neutral efflux out of the ion thruster. The charge exchange collisions between beam ions and these neutral propellant atoms are inevitable. In the case of ground testing, the charge exchange collisions can also occur between beam ions and atoms of the residual gas in the test facility. An important issue in the prediction of ion engine lifetime is the influence of the ground test facility on the accelerator grid erosion processes. In other words, it is necessary to understand the erosion processes in order to interpret the results of ground tests and to predict the ion engine lifetime in space operation.

Experimental observations [1-3] have shown that the maximum accelerator grid erosion occurs at the geometric center between apertures for a hexagonal symmetry geometry two-grid accelerator system. Since the velocities of the charge exchange ions are negligible when they are created by charge exchange collisions, the charge exchange erosion pattern is eventually determined by the electric field in the deceleration region. Because of the positive space charge inside the ion beam, there is a potential gradient in the transverse direction. This potential gradient tends to force charge exchange ions out of the primary beam and into the geometric center between apertures. This is where the lowest potential occurs, and therefore the maximum sputtering erosion occurs at those locations. Many numerical and analog methods have been used to study the ion optics and the accelerator grid erosion caused by charge exchange ions. The problem with the methods developed during the 1960's and 1970's is that it was difficult to determine the downstream plasma boundary where the potential gradient is small. Therefore, it was difficult to accurately simulate the electric field in the region downstream of the accelerator grid where most of the charge exchange collisions occur.

In 1990, at the 21st International Electric Propulsion Conference, we presented our direct particle simulation numerical code for the simulation of the ion optics and charge exchange collisions for a single aperture of a two grid system (two-dimensional axisymmetric model) [4]. The simulation model uses the Particle-In-Cell (PIC) method for the ion flow and a Monte Carlo method for charge exchange collisions. However, to simulate a pitted erosion pattern like that observed in the experiments, a three-dimensional (3-D) simulation model is required to include the geometric effects of the hexagonal symmetry array of apertures which comprise the screen and accelerator grids. The 3-D model is also required to correctly simulate the electric field in the downstream region of the accelerator grid. The preliminary calculation results of our three-dimensional model was first given in Reference 5, and the direct quantitative comparisons of the results of our 2-D and 3- D models was given in Reference 6. However, those calculations were made with an assumed neutralization plane boundary condition and assumed neutral downstream plasma density. This paper will consider the sensitivity of the calculated downstream electric potential field and the

* Research Engineer, UTSI/CSTAR
** Research Engineer, Calspan/CSTAR, AIAA member
† Professor, Engineering Science & Mechanics, AIAA member

predicted erosion pattern to the choice of the assumed downstream boundary conditions and plasma density.

In the next section, we present a brief description of our 3-D model, and then an example calculation using this 3-D model will be given. A parametric study of the effects of the downstream boundary conditions on the electric field in the downstream region and the erosion rate of the accelerator grid was carried out using our 2-D model. The 2-D model was chosen for this study because it requires significantly less computer time and is less expensive to run than the 3-D model.

II. 3-D Simulation Model

Ion optics

To simulate the electrostatic problem, the Poisson equation

$$\nabla^2\phi = -\frac{\rho}{\epsilon_o} \qquad (1)$$

is to be solved over the computational domain shown in Figs. 1 and 2, where ϕ is the electric potential, ρ is the charge density, and ϵ_o is the permittivity of free space. The cross section of the computational domain is chosen as small as possible: a 30 degree by 60 degree right triangle. The computational domain in the transverse direction is subdivided into smaller nonuniform triangular cells. The finite difference equations for Eq. (1) are derived using Winslow's scheme [7]. The Particle-In-Cell (PIC) method is used to determine the particle charge which appears on the right-hand side of Eq. (1). The PIC method utilizes a large number of simulation particles to simulate the charge flow. Each simulation particle represents a large number of ions and carries a corresponding electrical charge. The typical simulation procedure of the PIC method consists of the following principal steps:

1. Assign particle charges to the mesh.
2. Solve Poisson's equation on the mesh.
3. Obtain the mesh-defined electric field and interpolate forces at particle positions.
4. Move each of the simulation particles.

In our particular problem, the procedure includes the injection of new particles from an upstream plasma boundary at each time step and the calculation of the sputtering which occurs when an ion strikes a grid surface. Further details of the PIC method for the nonuniform triangular mesh are given in Reference 6.

Charge Exchange Collisions and Sputtering

Charge exchange collisions between fast moving beam ions and slow neutral particles are the principal cause of accelerator grid erosion. Most of those charge exchange ions which reach the accelerator grid and cause the grid erosion are produced between the downstream surface of the accelerator grid and the downstream plasma boundary. Because of the existence of an electric field, the charge exchange collision rate is both energy dependent and time dependent.

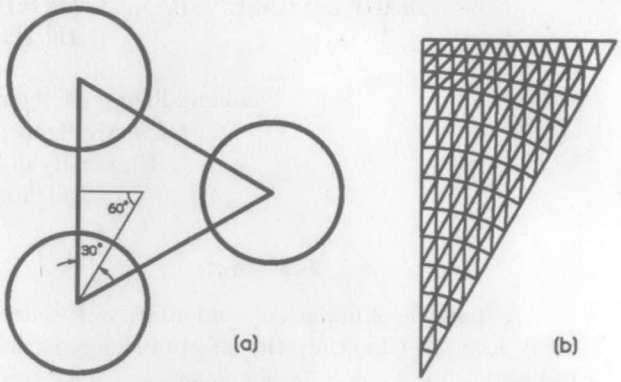

Figure 1: *Minimum cell computational cross-section for a hexagonal aperture grid (a), and nonuniform triangular mesh on this minimum cell (b), for a screen grid open fraction of 0.67.*

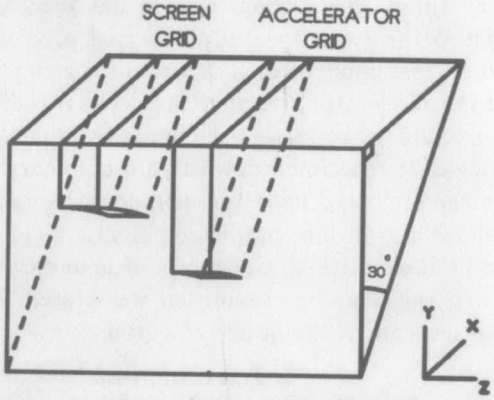

Figure 2: *View of the entire three-dimensional, wedge-shaped computational domain. Ion flow is from left to right.*

Therefore, we used a null collision Monte Carlo technique to simulate this time dependent charge exchange collision. The essence of this technique is that it accounts for the change in the charge exchange collision rate as an ion particle is accelerated during a computational timestep. The charge exchange rate for xenon, as a function of velocity, was obtained from Reference 25. For simplicity, the background neutral gas was assumed to have a constant density throughout the computational domain. Details of the Monte Carlo simulation procedure in the code are given in References 4 and 5.

Finally, sputtering rates for xenon ions impinging on a molybdenum surface were obtained from Reference 8. It was assumed that the sputtering process was independent of the angle of incidence of the ion.

III. Example Computation

Calculations were performed for operation of the ion thruster with xenon propellant, one of the propellants of choice for an actual space mission. It was assumed that a neutral plasma exists at the upstream boundary of the computational domain, which has an ion density of $1.\times10^{17}$ m^{-3}, a mean extracted ion ve-

locity of 300. m/s, an ion temperature of 1000 K and an electron temperature of 1.5 eV. The plasma potential is assumed to be at 1828 V, the screen grid is at a potential of 1800 V, the accelerator grid is at a potential of -510 V and the downstream boundary is at a potential of 0 V (the neutralization plane). Screen and accelerator grid hole diameters are 1.91 mm and 1.14 mm, respectively, with a 0.51 mm gap between apertures, grid thicknesses of 0.51 mm each, and a distance of 2.57 mm between two adjacent aperture centers, corresponding to a screen grid open fraction of 0.67.

Other than the propellant ions and the electrons, the only other species that was taken into account in the code was the neutral propellant atom. It is obvious that the higher background neutral gas density in the ground test facility, compared to space conditions, may enhance the charge exchange collisions. These collisions between fast beam ions and slow moving residual neutral atoms will provide additional slow moving charge exchange ions, and the grid erosion rate will increase. At the present time, we have assumed that the number density of these background neutral particles is constant throughout the computational domain. Actually, it is only the neutral gas density inside of the ion beam between the downstream side of accelerator and plasma boundary that is important to the accelerator grid erosion, since the most of the charge exchange ions which reach the accelerator grid and cause grid sputtering are created in this region. Therefore, the constant neutral gas density is actually assumed for the downstream region between the accelerator grid and the downstream plasma boundary.

The main purpose of this paper is to study how accelerator grid erosion is affected by hexagonal symmetry geometry apertures and the choice of downstream boundary conditions. Therefore, only electric potential contours and the downstream side of the accelerator grid erosion contours will be discussed. For results of the previous, 2-D axisymmetric computations and the preliminary 3-D calculations, we refer the reader to References 4,5 and 6.

Electric Potential Contours

The electric potential contours at different transverse cross-sections along the thruster axis are shown in Fig. 3. To aid in the visual interpretation of these results, each of following figures is a composite of six of the basic computational cross-section, arranged symmetrically around the geometric center of three adjacent apertures (thus, each of the three corners of the equilateral triangles constitutes one one-sixths of an aperture cross-section).

Fig. 3a shows the potential contours 0.05 mm upstream from the screen grid. The electric potential gradient shown in this figure focuses the beam ions through the screen grid aperture. A set of typical electric potential contours inside the screen grid aperture is shown in Fig. 3b. It can be seen that the beam ions are continuously focused through the apertures and the potential gradient in the transverse direction is much greater than in the upstream region of the screen grid.

The transverse electric potential gradient changes its direction somewhere between the screen grid and the accelerator grid. This is shown in the progression of Figs. 3c, 3d, and 3e proceeding from 0.3825 mm, 0.2550 mm, and 0.1275 mm upstream from the accelerator grid. In Fig. 3c, the electric potential gradient is about 378 Volts and tends to focus beam ions toward the axis of the apertures. While the electric potential gradient shown in Fig 3d still shows the tendency to force the ions toward the axis of the apertures, the potential gradient has dropped to about 91 Volts. The complete opposite electric potential gradient appears in Fig. 3e because it is closer to the accelerator grid and because of the existence of the positive ions. Therefore, the transverse electric field changes its direction from focusing to diverging the ion beams at a position somewhere between the screen and accelerator grids.

A set of typical electric potential contours inside the accelerator grid aperture is shown in Fig. 3f. The potential gradient does not have a very large value. Thus, if charge exchange ions are created inside the aperture, they will not gain sufficient energy to cause much damage to the accelerator grid.

The transverse electric potential contours in the region downstream of the accelerator grid are shown in Figs. 3g through 3j. As shown in these figures, the downstream electric fields influence the performance of the thruster in two ways. First, the transverse electric field tends to diverge the ion beams which results in decreasing the vector thrust of the engine. Second, the effect on slow charge exchange ions by such electric fields is to accelerate these ions back upstream toward the grids and to focus them onto the geometric centers between apertures. This accounts for the pitted erosion spots that are observed to occur between apertures, and explains the sputtering erosion patterns observed on the downstream surface of the accelerator grid in the experiments [1,2,3].

Sputtering Contours of the Accelerator Grid

The erosion pattern of the accelerator grid is primarily determined by the electric field in the downstream deceleration region (between the accelerator grid and the plasma boundary), because charge exchange ions are relatively stationary when they are created by charge exchange collisions. Therefore, charge exchange ions which are created in the downstream deceleration region inside the ion beam plume will be accelerated back toward the accelerator grid and cause sputtering erosion to occur there. To quantify this ero-

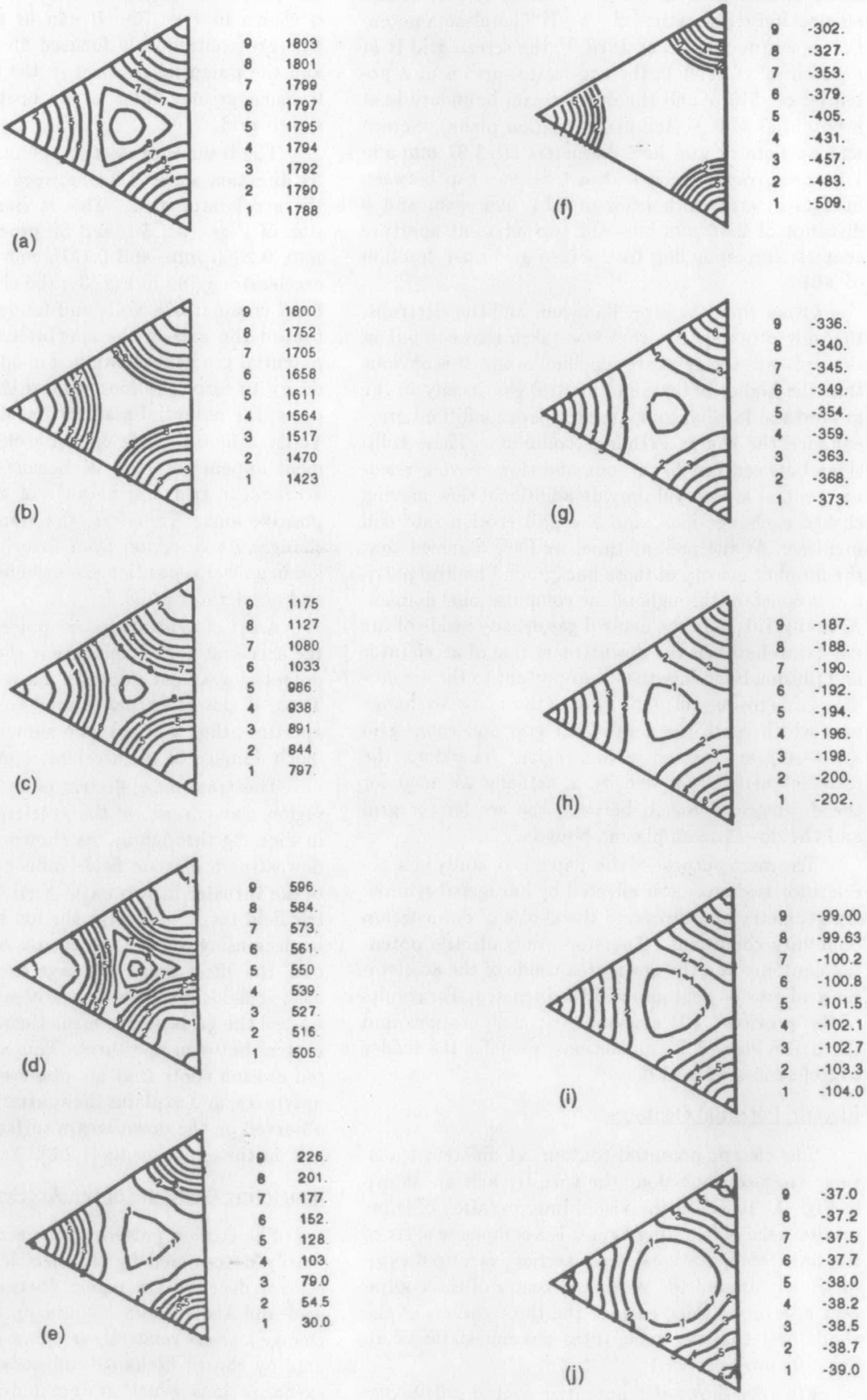

Figure 3 *Electric potential contours at different transverse cross-section along the thruster axis.*

sion rate, the energy-dependent sputtering yield for xenon atoms on molybdenum was obtained from a General Mills Report [8]. Fig. 4 shows the resulting number of molybdenum atoms sputtered per unit area for the downstream surface of the accelerator grid (to aid in the visual interpretation, several cross-sections are shown together). In Fig. 4, the concentration of sputtering between grid apertures is clearly visible. This figure has been shown in our previous paper [6], where a more complete discussion can be found.

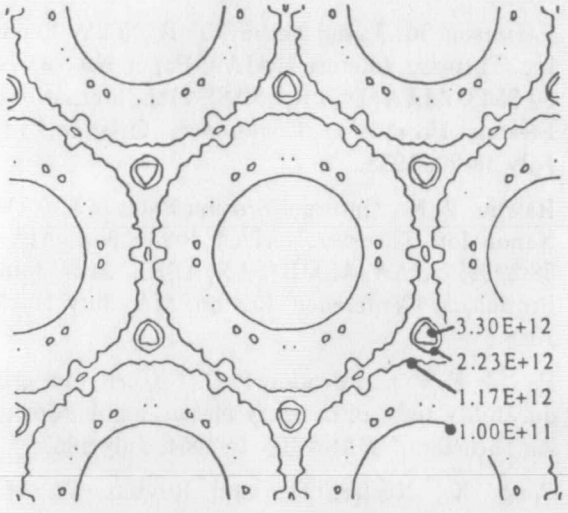

Figure 4: *Sputtering contours on the downstream surface of the acceleraotr grid (values are number of atoms per square meter per 5.44 μsec). Note the concentration of sputtering between apertures.*

As discussed above, the charge exchange grid erosion is determined by the downstream electric field. Therefore, we must determine how the assumed downstream conditions in our simulation model influence the electric potential field and, therefore, the erosion rate of the accelerator grid. In the next section we investigate the effect of different downstream boundary conditions using our two-dimensional model, since it requires significantly less computer time than the three-dimensional model.

Parametric Study of Downstream Conditions

The shape and location of the downstream plasma boundary is important to explain the accelerator grid charge exchange erosion patterns observed in the experiments. Therefore, by choosing different downstream boundary conditions and varying the distance between the accelerator grid and the assumed boundary position, the sensitivity of the downstream electric potential field and the shape and location of the potential contours can be assessed.

The geometry and plasma conditions in the following calculations were chosen to correspond to the experimental configuration used by Patterson and Verhey [1]. The screen and accelerator grid radii are 0.95 and 0.55 *mm*, respectively. The outside radius of the computational domain is 1.11 *mm*, yielding the desired screen open fraction of 0.67. The thickness of both grids is 0.38 *mm*, and distance between two grids is 0.76 *mm*. The plasma boundary is at 0.095 *mm* upstream from the screen grid. It is assumed that a neutral plasma exists at the upstream boundary of the computational domain with an ion density of $1.34\times10^{18}\mathrm{m}^{-3}$, an ion temperature of 1000 K, a mean ion extraction velocity of 400 m/s, and an electron temperature of 1.5 eV. The plasma potential is assumed to be at 1544 V, 28 V more positive than the screen grid which is at a potential of 1517 V. The accelerator grid is at a potential of -331 V. Downstream plasma conditions are taken to be equal to those of the upstream plasma, except for the ion density. The neutral gas density is assumed uniform throughout the computational domain at a density of $5\times10^{18}m^{-3}$, and represents a residual facility background, rather than efflux from the thruster.

Several choices can be made for the downstream boundary condition. A fixed potential can be assumed at the downstream end of the computational domain if this potential is known. It may also be assumed that the electric field approaches zero at the boundary. This corresponds to setting the potential derivative equal to zero. It may also be assumed that the plasma approaches charge neutrality at the boundary. This corresponds to setting the second derivative of potential equal to zero. Each of these assumptions has been used in the calculations discussed below.

Figs. 5 and 6 show electric potential contours calculated using different downstream boundary conditions. In both figures the boundary conditions are: (a) electric potential equals zero, $\phi = 0$; (b) electric field equals zero, $\partial\phi/\partial z = 0$; and (c) the second derivative of electric potential equals zero, $\partial^2\phi/\partial z^2 = 0$. The assumed boundary positions in Fig. 5 and Fig. 6 are located at 3 *mm* and 5 *mm* downstream from the accelerator grid, respectively. Comparing Figs. 5 and 6, it can be seen that if the assumed boundary is too close to the accelerator grid, the shape of the potential contours near the boundary is sensitive to which boundary condition is chosen. However, the shape and location of the potential contours and the peak value of the potential hill are not sensitive to the different boundary conditions if the assumed boundary position is far enough from the accelerator grid, as shown in Fig. 6.

Figs. 7 an 8 show the erosion rates which result from using the different downstream boundary conditions. Figures 7 and 8 correspond to Figures 5 and 6, respectively. In both figures, again, the boundary conditions are: (a) electric potential equals zero, $\phi = 0$; (b) electric field equals zero, $\partial\phi/\partial z = 0$; and (c) the second derivative of electric potential equals zero, $\partial^2\phi/\partial z^2 = 0$.

In Fig. 7, case (a) is different from the other two cases, because the shape of the potential contours for case (a) is different than cases (b) and (c), as shown in Fig. 5. Only those charge exchange ions which are created in the region between the accelerator grid and the upstream side of the potential hill will be accelerated back to the grid and cause sputtering erosion. Therefore, when the potential contours are similar, as shown in Fig. 6, it is expected that the erosion rates will not show significant differences, which is confirmed by Fig. 8.

Fig. 9 shows the calculated electric potential contours for different downstream distances between the accelerator grid and the assumed boundary position. Three cases are shown in the figure with distances of: (a) 3 *mm*; (b) 4 *mm*; and (c) 5*mm*. The boundary condition for all three cases is that the electric potential is set to zero. Fig. 10 shows similar comparisons but with a different downstream boundary condition: the second derivative of electric potential is set equal to zero. For the assumption that the potential is equal to zero, it can be seen, from Fig. 9, that the shape of the electric potential contours varies when the distance between the accelerator grid and the assumed boundary position changes. These differences in the potential fields will result in different erosion patterns. Fig. 11 shows the erosion rates for three different cases corresponding to the ones in Fig. 9. However, the shape of the potential contours are not very sensitive when the distance between accelerator grid and the assumed boundary position is changed, as shown in Fig. 10. Thus, for the same reason as discussed for Fig.8, the erosion patterns corresponding to the three cases in Fig. 10 will not show significant differences, as shown in Fig. 12.

IV. Conclusions

The accelerator grid erosion pattern is primarily determined by the downstream deceleration electric potential field. The three-dimensional model has shown how the observed pitted erosion patterns in the hexagonal symmetry geometry accelerator grid system are generated by the downstream electric field. The shape and the location of the downstream plasma potential contours is not sensitive to what boundary condition is chosen and where the assumed boundary is located, if the assumed downstream boundary is far inside the downstream plasma region. Therefore, the predicted accelerator grid erosion patterns and erosion rates will not be sensitive to the assumed downstream boundary condition used in the simulation model, if the assumed downstream boundary is far inside the downstream plasma region. However, it should be pointed out that this conclusion is based on a simulation which does not include a direct simulation of the neutralization process. To fully understand how the erosion process is influenced by the downstream plasma condition may require the detailed simulation of the neutralization processes and the downstream plasma.

Acknowledgment

This work was jointly supported by Boeing Defense and Aerospace Company, Seattle, WA and the University of Tennessee-Calspan Center for Space Transportation and Applied Research under NASA Grant NAGW-1195. The contract monitor was Dr. J. S. Meserole.

References

[1] Patterson, M. J. and Verhey, T. R.,"5-kW Xenon Ion Thruster Lifetest," AIAA Paper No. AIAA 90-2543, AIAA/DGLR/JSASS 21th International Electric Propulsion Conference, Orlando, FL, July 18-20, 1988.

[2] Rawlin, V. K., "Internal Erosion Rates of a 10-kW Xenon Ion Thruster," AIAA Paper No. AIAA 88-2912, AIAA/ASME/SAE/ASEE 24th Joint Propulsion Conference, Boston, MA, July 11-13, 1988.

[3] Pawlik, E. V. and Reader, P. D., "Accelerator grid durability tests of mercury electro-bombardment ion thrusters," NASA TN D-4054, July 1967.

[4] Peng, X., Keefer, D., and Ruyten, W. M., "Plasma Particle Simulation of Electrostatic Ion Thrusters," AIAA paper 90-2647, Orlando, Florida, July 1990.

[5] Peng, X., Ruyten, W. M., and Keefer, D., "Monte Carlo Simulation of Ion-neutral Charge Exchange Collisions and Grid Erosion in an Ion Thruster,"AIAA paper 91-0607, Reno, Nevada, January 1991.

[6] Peng, X., Ruyten, W. M., and Keefer, D., "Comparison of 2-D and 3-D Models of Grid Erosion in an Ion Thruster," AIAA paper 91-2120, Sacramento, California, June 1991.

[7] Winslow, A. M. "Numerical Solution of the Quasilinear Poisson Equation in a Nonuniform Triangular Mesh," J. Comp. Phys. 2, 149–172 (1967).

[8] *Sputtering Yield Data in the* 100 – 600 *eV Energy Range*, General Mills Report 2309, July 15, 1962.

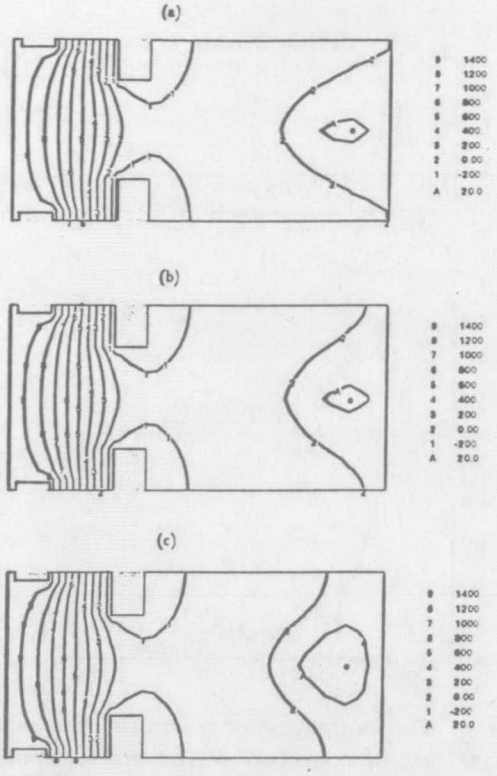

Fig. 5 *Computed electric potential contours for different downstream boundary conditions: (a) $\phi_e = 0$, (b) $(\frac{\partial \phi}{\partial x})_e = 0$, and (c) $(\frac{\partial^2 \phi}{\partial x^2})_e = 0$. The distance between the accelerator grid and assumed boundary position is 3 mm.*

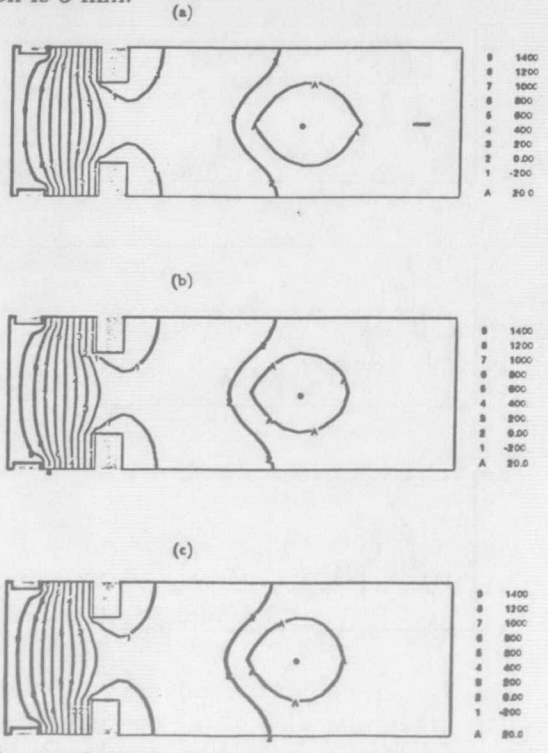

Fig. 6 *Computed electric potential contours for different downstream boundary conditions: (a) $\phi_e = 0$, (b) $(\frac{\partial \phi}{\partial x})_e = 0$, and (c) $(\frac{\partial^2 \phi}{\partial x^2})_e = 0$. The distance between the accelerator grid and assumed boundary position is 5 mm.*

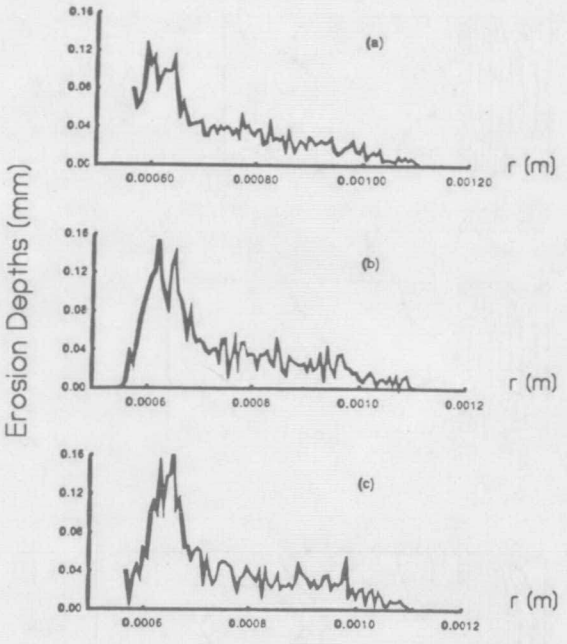

Fig. 7 *Comparison of computed erosion depths per 1000 hrs of operation of the downstream accelerator grid surface as a function of radius for different downstream boundary conditions: (a) $\phi_e = 0$, (b) $(\frac{\partial \phi}{\partial x})_e = 0$, and (c) $(\frac{\partial^2 \phi}{\partial x^2})_e = 0$. The distance between the accelerator grid and assumed boundary position is 3 mm.*

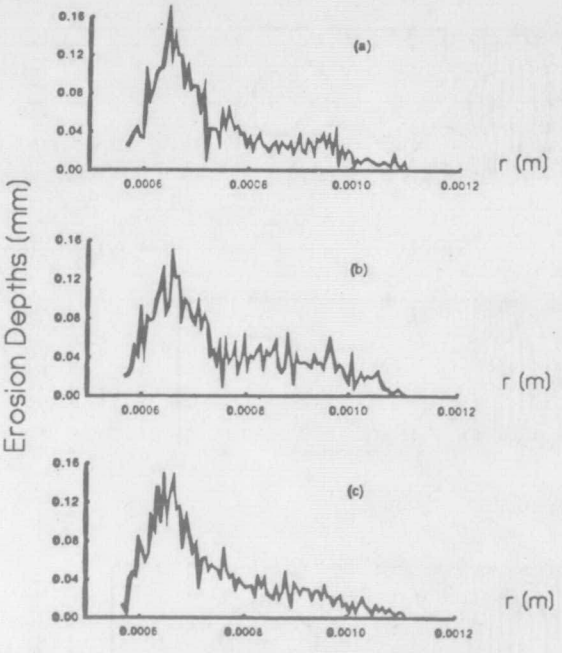

Fig. 8 *Comparison of computed erosion depths per 1000 hrs of operation of the downstream accelerator grid surface as a function of radius for different downstream boundary conditions: (a) $\phi_e = 0$, (b) $(\frac{\partial \phi}{\partial x})_e = 0$, and (c) $(\frac{\partial^2 \phi}{\partial x^2})_e = 0$. The distance between the accelerator grid and assumed boundary position is 5 mm.*

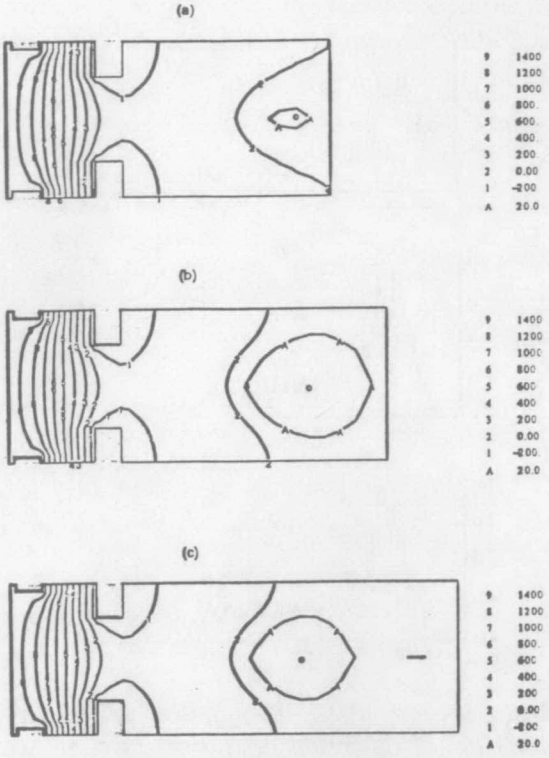

Fig. 9 *Comparison of computed electric potential contours with the distance between the accelerator grid and downstream boundary equal to: (a) 3 mm, (b) 4 mm, and (c) 5 mm. The assumed boundary condition is:* $\phi = 0$.

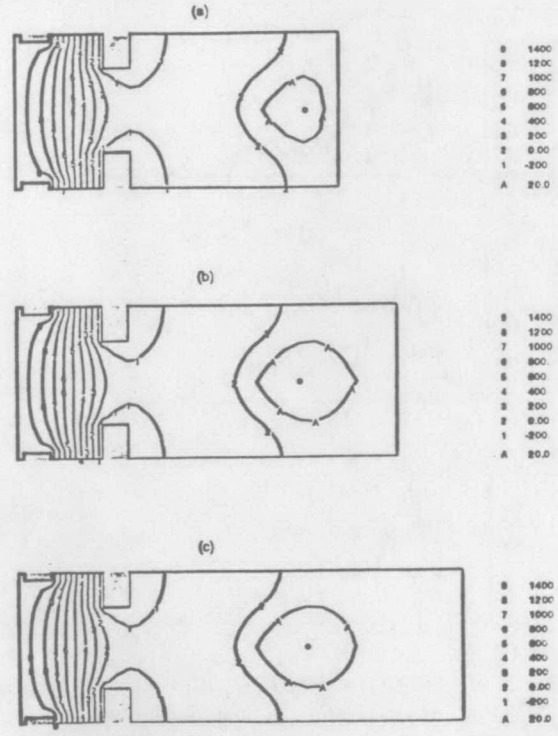

Fig. 10 *Comparison of computed electric potential contours with the distance between the accelerator grid and downstream boundary equal to: (a) 3 mm, (b) 4 mm, and (c) 5 mm. The assumed boundary condition is:* $(\frac{\partial^2 \phi}{\partial x^2})_e = 0$.

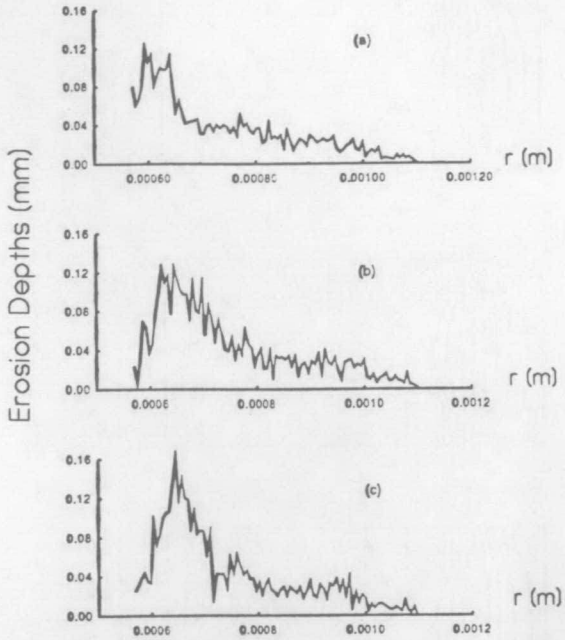

Fig. 11 *Comparison of computed erosion depths per 1000 hrs of operation of the downstream accelerator grid surface as a function of radius for different distance between the accelerator grid and assumed boundary position: (a) 3 mm, (b) 4 mm, and (c) 5 mm. The assumed downstream boundary condition is:* $\phi = 0$.

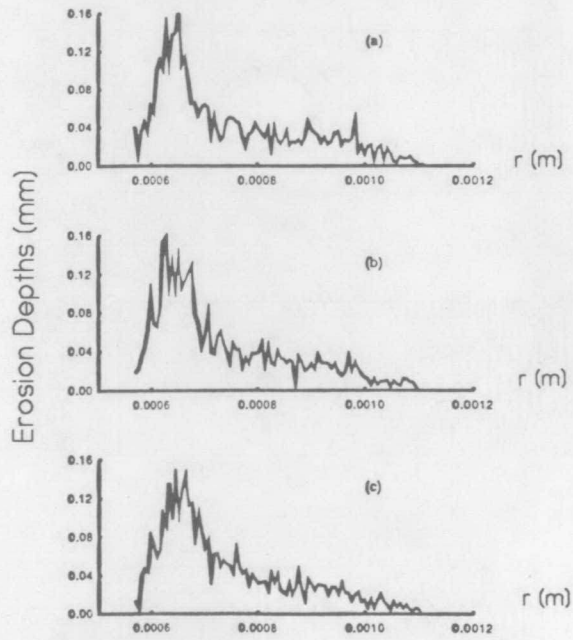

Fig. 12 *Comparison of computed erosion depths per 1000 hrs of operation of the downstream accelerator grid surface as a function of radius for different distance between the accelerator grid and assumed boundary position: (a) 3 mm, (b) 4 mm, and (c) 5 mm. The assumed downstream boundary condition is:* $(\frac{\partial^2 \phi}{\partial x^2})_e = 0$.